Bioactive Materials 6 (2021) 1150–1162

Contents lists available at ScienceDirect

Bioactive Materials

journal homepage: http://www.keaipublishing.com/biomat

Viscosity and degradation controlled injectable hydrogel for esophageal endoscopic submucosal dissection

Chaoqiang Fan[a,b,1], Kaige Xu[b,1], Yu Huang[a,1], Shuang Liu[a], Tongchuan Wang[a], Wei Wang[a], Weichao Hu[a], Lu Liu[a], Malcolm Xing[b,*], Shiming Yang[a,**]

[a] Department of Gastroenterology, Xinqiao Hospital, Army Medical University, NO.183, Xinqiao Street, Shapingba District, Chongqing City, 400037, People's Republic of China

[b] Department of Mechanical Engineering, Biochemistry and Medical Genetics, University of Manitoba, Winnipeg MB, R3T 2N2, Manitoba, Canada

ARTICLE INFO

Keywords:
Injectable hydrogel
Controllable gelation and viscosity
Esophageal submucosal liquid cushion
Early esophageal cancer
Pig model

ABSTRACT

Endoscopic submucosal dissection (ESD) is a common procedure to treat early and precancerous gastrointestinal lesions. Via submucosal injection, a liquid cushion is created to lift and separate the lesion and malignant part from the muscular layer where the formed indispensable space is convenient for endoscopic incision. Saline is a most common submucosal injection liquid, but the formed liquid pad lasts only a short time, and thus repeated injections increase the potential risk of adverse events. Hydrogels with high osmotic pressure and high viscosity are used as an alternate; however, with some drawbacks such as tissue damage, excessive injection resistance, and high cost. Here, we reported a nature derived hydrogel of gelatin-oxidized alginate (G-OALG). Based on the rheological analysis and compare to commercial endoscopic mucosal resection (EMR) solution (0.25% hyaluronic acid, HA), a designed G-OALG hydrogel of desired concentration and composition showed higher performances in controllable gelation and injectability, higher viscosity and more stable structures. The G-OALG gel also showed lower propulsion resistance than 0.25% HA in the injection force assessment under standard endoscopic instruments, which eased the surgical operation. In addition, the G-OALG hydrogel showed good *in vivo* degradability biocompatibility. By comparing the results acquired via ESD to normal saline, the G-OALG shows great histocompatibility and excellent endoscopic injectability, and enables create a longer-lasting submucosal cushion. All the features have been confirmed in the living both pig and rat models. The G-OALG could be a promising submucosal injection agent for esophageal ESD.

1. Introduction

Esophageal cancer is a leading malignant tumor in terms of morbidity and mortality due to emerging issues in food safety and diet, and the changes of environment and weather [1,2]. Endoscopic mucosal resection (EMR) has been widely used to treat early esophageal cancer and precancerous lesions. However, most early lesions are flat, thus endoscopic submucosal dissection (ESD) was introduced as an efficient and a minimally invasive way to separate the malignant from normal tissue. ESD is an endoscopic resection procedure, first reported by Gotoda T's team [3] in 1999, and the technique has become mature in the management of gastrointestinal cancers. Recently, ESD, which enables complete remove the lesions that are too large for en-bloc endoscopic mucosal resection (EMR), has been developed [4]. However, it is a time-consuming operation with difficulty and risk even greater than EMR. Thus, as for submucosal fluid cushion in esophagus during section, keeping a desired height and maintaining an appropriate time is critical for a successful operation. It has become an indispensable step to inject the liquid into the loose submucosa to form the submucosal cushion [5].

Recently, as submucosal liquid cushion, normal saline (NS) is a most used agent for injection; however, NS can maintain only a short time of about 3 min due to fast diffusion of small molecules, low viscosity and isotonic crystalloid solution nature. Multiple injections are always needed in a complete operation, which raises the concern of the potential surgical risks such as the prolonged operation time, the

Peer review under responsibility of KeAi Communications Co., Ltd.
* Corresponding author.
** Corresponding author.
E-mail address: nanoxing@gmail.com (M. Xing).
[1] Contribute equally to this article.

https://doi.org/10.1016/j.bioactmat.2020.09.028
Received 10 August 2020; Received in revised form 26 September 2020; Accepted 27 September 2020

Table 1
Main materials' features for submucosal injection.

Injection solution	Cushion duration	Cost	Advantage	Disadvantage
NS [7]	+	Low	Readily accessible; Most affordable; Non-toxic	Poor submucosal elevation; Fast diffusion
HA [8]	+ + + +	High	Widely available	Expensive; inducing the growth of residual tumorous cells; High injection resistance
3.75% SC [9]	+ +	Low	Readily accessible	Tissue damage
50% DW [9,10]	+ +	Low	Readily accessible	Tissue damage; Risk of post-polypectomy coagulation syndrome
Eleview® [11]	+ + + +	High	Non-toxic	Expensive
HPMC [12,13]	+ + +	Moderate	Non-toxic	Possible risk of antigenic reactions; Tissue damage
SG [14]	+ + + +	Moderate	Non-toxic	Hypersensitivity reaction
FM [13,15]	+ + + +	High	Non-toxic; Hemostatic effect	Contamination with some viruses
HES [16]	+ + + +	Moderate	Non-toxic	High injection resistance
GF [13]	+ + +	Moderate	Non-toxic	Produce excessive smoke during ESD; High injection resistance
AB [13,17,18]	+ + +	Low	Widely available; Non-toxic	Poor visual field of operation; High injection resistance; Easy to clot in syringe
PCCH [19]	+ + +	Low	Non-toxic	Complexity in preparation and using
CD [20]	+ + +	Moderate	Non-toxic	leak out of the pinhole after injection
PLGA [21]	+ + +	Moderate	Non-toxic	Low degradation rate
NSA [22–24]	+ + + +	Low	Non-toxic	High injection resistance; Uneven thickness of the liquid cushion; Unexplained mucosal shrinkage; High incidence of adverse event related to injection solution
ARSA [25]	+ +	Low	Non-toxic	Poor submucosal elevation
Our G-OALG	+ + + +	Low	Non-toxic	Non

NS: normal saline; HA: Hyaluronic acid; SC: Sodium chloride; DW: Dextrose water; Eleview®: Aries Pharmaceuticals, San Diego, California, USA. HPMC: Hydroxypropyl methylcellulose; SG: Succinylated gelatin; FM: Fibrinogen mixture; HES: Hydroxyethyl starch; GF: Glycerin fructose; AB: Autologous blood; PCCH: photo-crosslinkable chitosan hydrogel; CD: chitosan derivative; PLGA: poly lactic acid-co-glycolic acid thermogel. NSA: Natural sodium alginate; ARSA: Artificial reconstructive sodium alginate; G-OALG: Gelatin-Oxidized alginate.

correspondingly rising dosage of anesthetic drugs, and the potential risk of anesthesia. Therefore, a more durable and viscous submucosal liquid cushion has been an intense interest. Biomaterials injection lifts the lesion and separates it from the muscular layer, thereby reduces thermal injury and the risks of perforation and bleeding, thus facilitates en-bloc resection [6].

The alternates, such as hyaluronic acid (HA), hypertonic glucose, hydroxypropyl methylcellulose, glycerin fructose, for submucosal injection with high osmotic pressure and/or high viscosity have been explored and evaluated. They were summarized in Table 1.

As one of the popular ESD materials, HA has a longest-lasting fluid cushion, relative high successful en-bloc resection and low perforation complication rates [26–28]. However, HA is expensive and may induce tumor growth factors to promote the proliferation of tumor cells around the wound surface [8]. In addition, the liquid pad of HA is less effective in the scar area where the tube wall is weaker (esophagus, duodenum and colon), and the increased concentration is needed to maintain the pad for longer, which significantly increase the injection resistance and drug dosage. All these limits the clinical use of HA in ESD.

Sodium alginate (SALG) is a verified effective submucosal liquid by animal experiments [22,23]. However, several problems have been identified in clinics: too viscous, high injection resistance, uneven thickness of the liquid cushion, and unexplained mucosal shrinkage [23,29,30]. These phenomena are resulted from the absence of cationic recombination of natural SALG and its unstable viscosity in contact with the various environments of the digestive tract [31]. It can be physically ionic crosslinked rapidly at the presence of divalent cations [32]. However, the submucosal injection is hard to be controlled or operated since the gelation period is too short during cationic crosslinking; for example, rapid gelation in vitro results in excessive injection resistance, which is not convenient for endoscopic injection [33]. In addition, SALG does not promote efficient cell attachment, which leads to poor cell-material interactions [32,34]. Besides, studies in isolated pig stomachs have shown that the height of the hydrogel formed by mixing SALG with calcium or barium ions dropped very quickly [25]. In addition, a recent clinical study showed that although 0.6% SALG was slightly superior to 0.4% HA in terms of submucosal liquid cushion property, the incidence of adverse event related to submucosal injection solution was as high as 8.2% [24]. Therefore, we speculated that the viscosity and water retention of SALG hydrogel may still not be stable enough, which may be difficult to meet clinic requirements.

Recently, chitosan has been developed as materials for submucosal injection [35]. However, it is dissolvable under acid condition [36,37] In addition, chitosan has high percent amine groups, which may increase crosslinking density with oxidized alginate to form the hydrogel with relative higher stiffness or even brittle [37,38]. For example, pinhole leakage was reported after the injection of chitosan derivatives [20]. All these limits further application for submucosal liquid cushion.

Some submucosal injection materials degrade too slowly *in vivo* and have poor histocompatibility with the inclination to form foreign bodies of fibrous tissue wrapping [21]. Endoscopically injectable shear-thinning hydrogels synthesized by SALG and laponite showed a good endoscopic injectability and lasting mucosal liquid cushion, which contributed to the intestinal polyps resection [39]. However, laponite, as an inorganic ceramic material, is still unclear about the rate of degradation and the longer-term effects on local tissue when injected into a living organism.

An ideal submucosal injection should consider the following characteristics: safety, low cost, easy to obtain, facile to prepare and inject, able to maintain a long-lasting submucosal cushion for an operation, and no damage to the surrounding tissues [6,40]. All of these propelled us to consider a gel by combining with gelatin through a mild Schiff bonding with aldehyde modified alginate. Denatured from collagen, gelatin can be derived from diverse sources that cost effectively [41]. As the function and structure are closed to extracellular matrix, gelatin promotes cell adhesion [42,43]. Due to good biocompatibility and biodegradability [44], gelatin has relatively low antigenicity and relative short term degradation period [45,46]. Oxidized alginates with aldehydes (OALG) are a partially oxidized product of alginates which

can further be used to form covalent crosslinked hydrogel through Schiff's base formation with the reaction of free amine of lysine or hydroxylysine of gelatin. In addition, the relatively low abundance of free amine group in gelatin can control the overall crosslinking density, which makes the crosslinked hydrogel soft with controlled gelation and viscosity for ESD injection [47,48]. Therefore, all these benefits result in the OALG and gelatin can be promising candidate for submucosal liquid cushion.

To address the aforementioned concerns, here, we developed gelatin-oxidized alginate hydrogel (G-OALG) with higher performances in controllable injectability and gelation, higher viscosity and more stable structure than commercial EMR solution (0.25% HA) by rheological analysis. In addition, the G-OALG gel also showed lower propulsion resistance than 0.25% HA in the injection force assessment under standard endoscopic instruments, which eased the surgical operation. As well, the G-OALG hydrogel showed good *in vivo* degradability and biocompatibility in rat models. Most of the early lesions of the esophagus are flat, and most of them require ESD. ESD is a time-consuming operation, and the difficulty and risk in ESD are greater than in EMR, so the submucosal fluid cushion in esophagus is more important. Based on the above considerations, we compared the characteristics of G-OALG hydrogel with that of saline as esophageal submucosal injection in large animal model for the first time. (Schematic illustration).

2. Results and discussion

2.1. Characterizations of G-OALG hydrogels

The OALG was synthesized by reacting sodium alginate with sodium metaperiodate, which oxidized neighboring hydroxyl groups on carbon 2 and 3 to their dialdehyde derivatives [49]. Hydrogels can be prepared by crosslinking of gelatin with OALG. The mechanism of gelation was due to the Schiff base forming between amine residues of gelatin and aldehyde groups of OALG, then generated the imines [50] (Fig. 1A). The G-OALG hydrogels with different G/OALG mass ratios were prepared and compared in Table 2.

2.1.1. Hydrogel formation and gelation time

The test vial inverting method was first used to determine the gelation time of G-OALG with different mass ratios at 25 °C [51]; the magnetically stir bar stirring method was used to determine their gelation time at 37 °C [52]. Fig. 1C showed the gelation time of the G-OALG gels increased as the gelatin weight percent decreased at 25 °C. Except for gel of G40-OALG10 and G35-OALG15, all gels' gelation time was higher than ~6 min. As temperature increased to 37 °C, all gelation time was decreased but not significant changed (Fig. 1C), which may be because the relative higher temperature (37 °C) could not only accelerate the crosslinking rate but also break gelatin's physically self-entangling in chains [53–55]. For further verification, in the time sweep study of rheological analysis (Fig. 1D), the storage modulus (G′) and loss modulus (G″) were recorded with respect to time, the gelation time can be determined as crossover points of G′ and G″, where after G′ is higher than G''. It means gel formed. In the case of hydrogel G35-OALG15, the crossover point of G′ and G″ was obtained around 3 min, which was closed to the time that the preformed gel is injected and traveled through 2.3m-long guide tube in the clinic use (Fig. 1B and C). Among them, the crossover point at 37 °C was 23s ahead of that at 25 °C (Fig. 1D), which is corresponding to the ahead time of 19 ± 3s in Fig. 1C. On the course of the gelation, the G-OALG hydrogel could keep a low viscosity in a semi gel-liquid like (G" > G′) for the first 3 min after mixing. The solution gradually formed a solid gel (G' > G″) after injection to maintain a stable height of the submucosal liquid pad.

2.1.2. FTIR spectra of OALG, alginate, G35-OALG15 gel and gelatin

The FTIR spectrum of gelatin indicated the characteristic absorption bands at 1630 cm^{-1}, and 1540 cm^{-1} which are assigned to the C═O stretching vibration (amideI), and N–H bending vibration (amide II); while the band at 1220 cm^{-1} is the C–N stretching vibration [56,57]. The spectrum of sodium alginate demonstrated that the absorption bands around 1600 cm^{-1}, 1416 cm^{-1}, and 1306 cm^{-1} are attributed to the stretching vibrations of asymmetric and symmetric bands of carboxylate anions, respectively [58]. Moreover, FTIR spectrum of OALG showed a new characteristic peak at 1730 cm^{-1} (C═O), which was resulted from that the sodium metaperiodate was not completely consumed during oxidation since the hemiacetal formation between oxidized and unoxidized alginate residue. The symmetric vibration of aldehyde at 1735 cm^{-1} was not detected, which was due to hemiacetal formation of free aldehyde groups [59,60]. However, the formation of aldehyde groups in OALG were confirmed by ^{1}H NMR. After crosslinking, the characteristic peak of aldehyde groups was disappeared, which suggested the G35-OALG15 gel was successfully crosslinked through the Schiff-base reaction between gelatin and OALG. Also, the spectrum of G35-OALG15 indicated the absorption bands at 1620 cm^{-1} and 1554 cm^{-1} due to C═N the stretching vibration from the formation of Schiff's base [61,62] (Fig. 1G).

2.1.3. ^{1}H NMR spectra of OALG and alginate in D_2O

As shown in Fig. 1F, ^{1}H NMR spectrum of alginate exhibited peaks ranging from ~3.4 to ~4.8 ppm that were corresponding to protons of guluronate (G) and mannuronate (M) units [63]. Among them, the H-2 and H-3 signals of neighbor hydroxyl groups on alginate at ~3.6 ppm weakened obviously, which was because the hydroxyl groups were oxidized to aldehydes groups. In addition, the spectrum of OALG showed two new signals at ~5.3 and ~5.6 ppm after oxidization, which were related to the hemiacetalic proton formed from aldehydes and their neighbor hydroxyl groups (Fig. 1E) [64]; also, the H-1 signal changed the position from ~3.6 ppm to ~4.0 ppm [65]. The above changes all confirmed the formation of aldehydes on OALG.

2.1.4. Injectable properties of G-OALG hydrogels

The G-OALG hydrogels maintained gel state in water when injected from the syringe immediately after 5 min of gelation. The gelation for 5 min led to a more stable structure than immediate injection out where a diffusion was found in the water (Movie S1 and S2, Supplementary information). The G-OALG hydrogels injected onto the dry glass surface also showed a good gel-formability (Movie S3, Supplementary information). Endoscopic injection needle (length: 2.3 m, internal diameter: 0.32 mm) showed convenient injectability after immediate mixing with semi-gel forming (Movie S4, Supplementary information). (Fig. 1$F_{1\text{-}4}$).

Supplementary data related to this article can be found at https://doi.org/10.1016/j.bioactmat.2020.09.028.

2.2. Evaluation of rheological properties of G-OALG hydrogels

The dynamic rheological properties of different composite hydrogels were evaluated by oscillatory rheology tests. The frequency sweep measurements for the hydrogels were expressed as storage modulus (G′) and loss modulus (G″) (Fig. 2A). For all groups of hydrogels, G′ was always higher than G″ and G′ showed lightly increased in the range of 0.1–100 rad/s, which can prove that the hydrogels were crosslinked and exhibited mechanical robust [66–68] (Fig. 2D). As shown in Fig. 2B, both gels of G35-OALG15 and G30-OALG20 were well maintained their gel structure (G' > G″) even under high shear strain sweep ($\gamma \geq 1000\%$); moreover, the G40-OALG10 also showed in gel state under shear strain $\gamma \geq 1000\%$, but its gel inner structure was starting about to be collapsed (G′ was decreasing, G″ was increasing sharply, and G′ and G″ were trend to be crossed nearly) as shear strain increasing continuously. However, other groups of gels showed some collapse (G' < G″). From this, G35-OALG15 and G30-OALG20 could be as potential submucosal cushion. Moreover, to analyze the influence of Gelatin and OALG weight ratios on viscosities, the shear viscosity as a

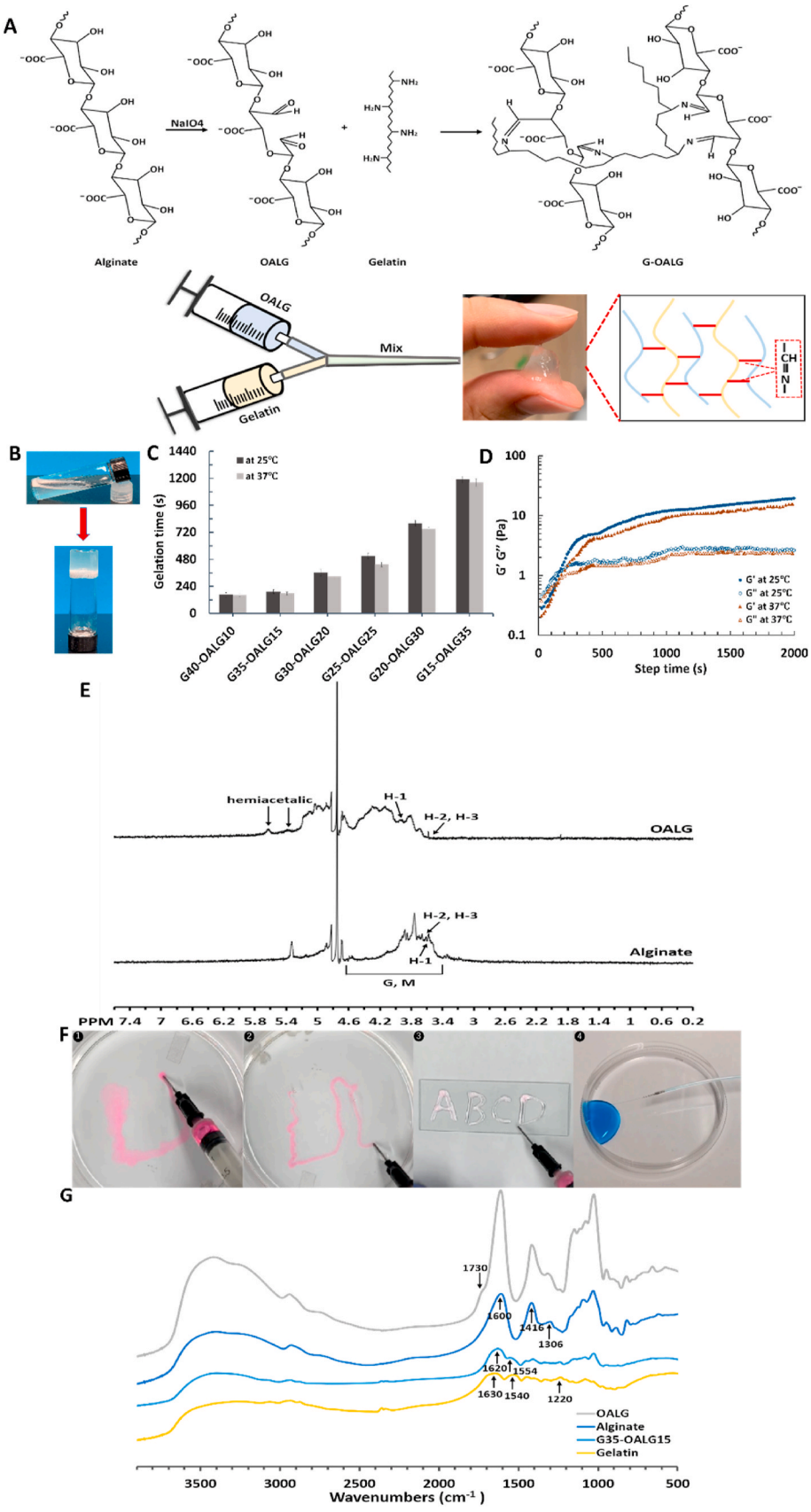

Fig. 1. Synthesis mechanism and characterization of G-OALG hydrogels. A. Synthesis of OALG from alginate with sodium periodic oxidation, and crosslinking of gelatin and OALG. B. Photo images of the formation of gelatin and OALG hydrogel before and after gelation; C. Gelation time of the G-OALG hydrogels with different G/OALG mass ratios at 25 °C and at 37 °C, respectively; D. Time dependence of storage modulus (G′) and loss modulus (G″) for the formation of G35-OALG15 hydrogel at both 25 °C and 37 °C. E. ^{1}H NMR spectra of OALG and alginate in D_2O. F. Injectable properties of G-OALG hydrogels. G. FTIR spectra of OALG, alginate, G35-OALG15 gel and gelatin.

function of the shear rate for G-OALG hydrogels were recorded as shown in Fig. 2C. As shear rate increased, all viscosities decreased, which suggested a typical shear-shinning behavior, an indicator for good injectable performance. As small weight ratio of G and OALG led to the declining the viscosity of hydrogels, which may be because of less crosslinking percent of gelatin. The G40-OALG10 showed highest viscosity at condition of low shear rate ($\leq 0.1\ s^{-1}$). It may be because in the G40-OALG10, all OALG have been consumed for crosslinking and

Table 2
G-OALG hydrogels with different weight ratios of gelatin to OALG and groups.

Final concentration (w/v%) in G-OALG hydrogel		Weight ratio of gelatin to OALG	Group
Gelatin	OALG		
4.0	1.0	40:10	G40-OALG10
3.5	1.5	35:15	G35-OALG15
3.0	2.0	30:20	G30-OALG20
2.5	2.5	25:25	G25-OALG25
2.0	3.0	20:30	G20-OALG30
1.5	3.5	15:35	G15-OALG35

In order to verify the performance of G-OALG hydrogels, we conducted the following characterization tests.

some gelatin remained free without crosslinking and was possible for physically self-entangling in chains which then increased the viscosity [69,70]. This physical chain-entanglement also may cause highest gelatin-contained hydrogel G40-OALG10 showed largest storage modulus G′, but not stable under high shear strain sweep ($\gamma \geq 1000\%$), which resulted in gel structure starting to be collapsed (G" increased sharply, Fig. 2B). In addition, all amines in gelatin may be consumed during crosslinking when the weight ratio of gelatin/OALG is 15:35, which may contribute to the shown lowest viscosity of the G15-OALG35 gel. As a submucosal cushion, the higher viscosity is a merit, since it can generate a long-lasting submucosal height that makes the performance of EMR more easily [71]. As considering both more stable in gels' structure and higher viscosity, and the gelation time was around 3 min to match the surgery procedures. Therefore, the gel of G35-OALG15 was used as a best option as submucosal cushion.

In addition, both G's of G25-OALG25 hydrogel under frequency and amplitude sweeps were less than hydrogel G30-OALG20, which further suggested that more gelatin in hydrogel increased the stiffness (Fig. 2E).

The characteristics of controllable gelatinization and shear thinning greatly convinced the endoscopic injection.

Furthermore, we studied the G35-OALG15 gel with different concentrations in the gelation and rheological properties, and compared them to commercial EMR solution (0.25% (w/v) HA) and NS. At first, we considered that G35-OALG15 gel with concentration of 50 mg/ml (5%, w/v) may cause relative higher propulsion resistance as injecting through the clinical guide tube, which may result in the undesired injection and increase the difficulty of surgical operation. Meanwhile, in order to reduce the cost and ease the surgical operating procedure, we conducted two more lower concentrations of G35-OALG15 gels (3% and 1.5%, w/v). As shown in Fig. 2F, the frequency sweep measurements for the 5%, 3%, and 1.5% G35-OALG15 gels were expressed as storage modulus (G′) and loss modulus (G″). By comparing to the 5% G35-OALG15 gel, both 3% and 1.5% G35-OALG15 gels also showed that G′ was higher than G″ and G′ increased in the range of 0.1–100 rad/s, which can prove that these two groups' gels were also crosslinked [66]. However, as concentrations were decreased from 5% to 1.5%, the G35-OALG15 gels showed less stability. For example, in the amplitude sweep measurements of 1.5% G35-OALG15 gel, though G′ was higher than G″, but the G′ was decreasing sharply under high shear strain sweep (Fig. 2G), which may because the lower concentration leads to less crosslinking density and formed very weak gel [72,73]. Thus, we may predict that the gel's at concentration lower than 1.5% may would not support a desired structure for EMR. In addition, all three concentrations G35-OALG15 gels showed injectable performance, all viscosities decreased as shear rates increased. As predicted, the viscosities decreased as concentrations decreased. As shown in Fig. 2I, the gelation time decreased as temperature or concentrations increased, but the gelation time decreased largely as concentrations increased. The concentrations played a dominant role in gelation time changes, which may be because lower concentrations resulted in less crosslinking density spatially but this spatially variation may not be changed largely by temperature; thus, the gelation time was not significant changed as temperature increased [74]. Therefore, summarized all above, with consideration of lower cost and less propulsion resistance through guide tube, the 1.5% G35-OALG15 (GO1) gel as a comparing group to 5% G35-OLAG15 (GO2) gel would be a candidate for further evaluation in injection force assessment.

When comparing our G35-OALG15 gels to commercial EMR solution (0.25% (w/v) HA), though the 0.25% HA showed injectability, but its viscosity was lower than our 5% and 3% G35-OALG15 gel's (Fig. 2H). As a submucosal cushion, the higher viscosity is desired, since it can generate a long-lasting submucosal height that makes the performance of EMR more easily [71]. Likewise, as another most used clinical EMR solution, the NS also showed lower viscosity which is one of reasons that the NS can maintain only a short time as submucosal liquid cushion and multiple injections are always needed to complete operation [75]. In addition, the 0.5% HA did not show stable performance in rheological studies (Fig. 2 F and G). For example, as shown in Fig. 2F, the G′ of 0.25% HA was lower than G″ at lower frequency ($\omega \leq 1.5$ rad/s). Also, in Fig. 2G, the G′ of the 0.25% HA was always lower than its G″ under shear strain sweep larger than 3.5% ($\gamma \geq 3.5\%$), which showed its unstable structure. All these may be because of the un-crosslinked liquid-like property and dilute character of the 0.25% HA [23,76]. Thus, we may predict that the 0.25% HA may not maintain stable and long-lasting submucosal cushion as EMR solution. In order to quantitate and compare the injection pressure data of our G-OALG hydrogels (GO1 and GO2) to the 0.25% HA and the NS, they were further evaluated by injection force assessment.

The injection forces of GO1 and GO2, 0.25% HA, and NS under standard endoscopic instruments has been simulated and assessed. The 5 ml of each sample was added to a 20 ml injection, which was injected with a 750 g weight pushing injector for 1 min, respectively. The volume of each sample flowing out of the endoscope needle was recorded and then made an assessment. The volumes of NS, GO1, GO2 and 0.25% HA was 4.5, 0.24, 0.1 and 0.04 ml, respectively. The results were shown in Fig. S1 (Supplementary information), and the detailed procedures were shown in Movie S5-S8 (Supplementary information).

Supplementary video related to this article can be found at https://doi.org/10.1016/j.bioactmat.2020.09.028

The results showed that the force required for GO1 and GO2 were more than NS and less than 0.25% HA, the NS almost had no viscosity under the standard endoscopic instruments, and the fluidity was very well. Compared to 0.25% HA, GO1 and GO2 were more easily injected into the submucosal layer with standard endoscopic instruments. However, the NS had the fastest dispersion speed in the submucosa. The GO1 and GO2 have good submucosal cushion effect after formation, which is beneficial to the operation of ESD.

2.3. Biocompatibility in rat

A cutaneous hillock about 2.0 cm in diameter was formed after G-OALG hydrogel (G35-OALG15: 1 ml, 50 mg/ml) was injected subcutaneously on the back of the rat. The next day, the cutaneous hillock decreased significantly and almost disappeared at the day 3 after the injection. Inflammatory responses, such as edema, redness and ulceration were not found at the injection site of all the rats, and the skin was soft and without any subcutaneous nodule at all time points after injection Fig. 3A. When the skin of the injection site was removed, a translucent bulge was found about 2.0 cm in diameter at day 0. The bulge became significantly smaller at day 1 and 3, and can not found at the day 5 and 7 after the injection (Fig. 3B). H&E staining showed the range of the G-OALG hydrogel under the skin of the rat at Day 0 and Day 1 (red circle), and we can see some of the local inflammatory cells at Day 0, which disappeared over the next few days. The G-OALG hydrogel had been almost completely absorbed at Day 3, Day 5, and Day 7, and no inflammation, fibrous encapsulation, and ulcers were

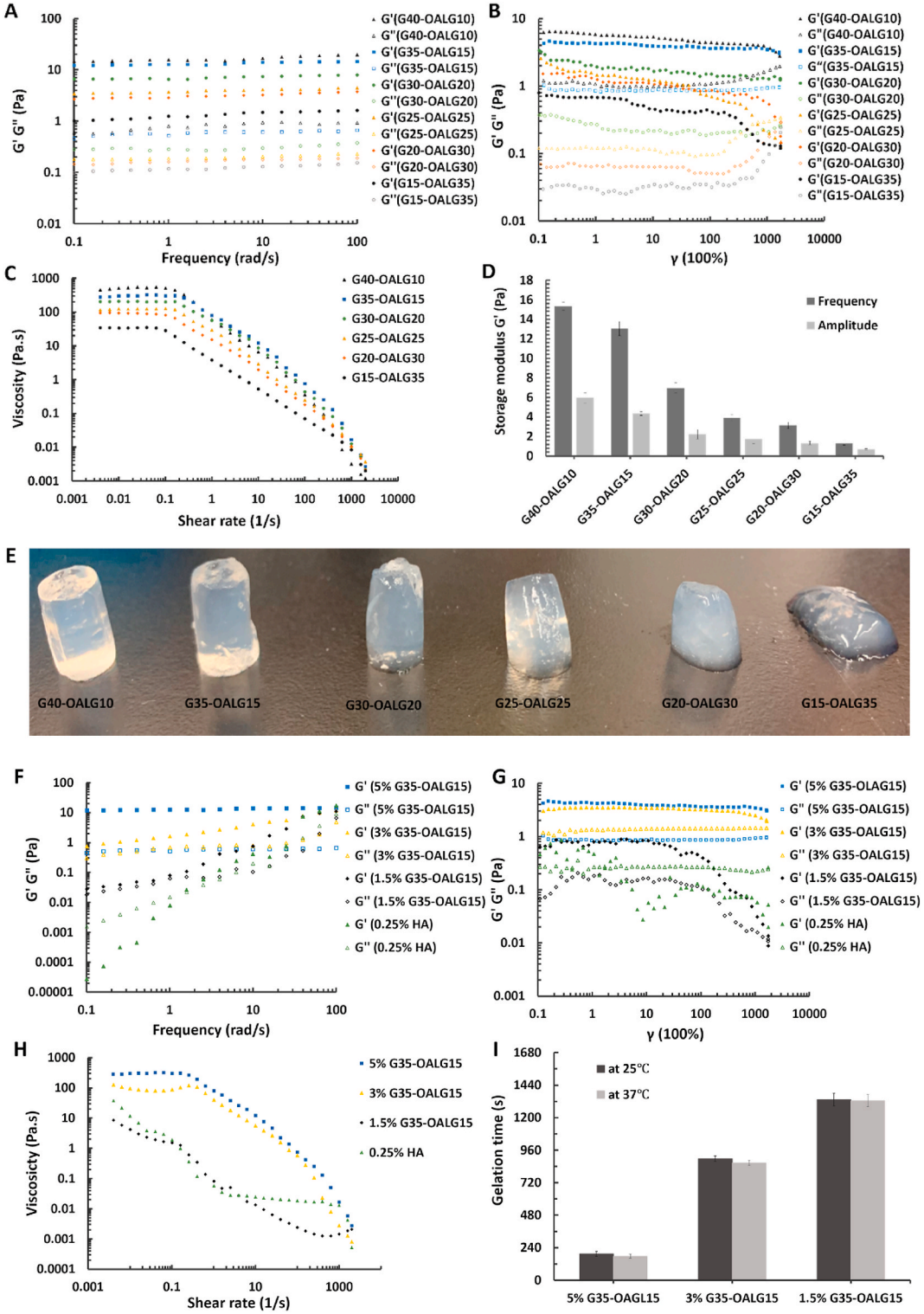

Fig. 2. Rheological properties of G-OALG hydrogels. A. Frequency dependence of storage modulus (G′) and loss modulus (G″) of hydrogels with different concentrations of gelatin and OALG; B. Amplitude dependence of G′ and G″ of different composite hydrogels; C. Viscosity as a function of the shear rate for different concentration hydrogels; D. Storage modulus G′ under frequency sweep (black) and amplitude sweep (grey) of the G-OALG hydrogels with different composites. E. Photo images of hydrogels with various gelatin/OALG composites. Rheological properties of G35-OALG15 hydrogels with different concentrations (5%, 3%, and 1.5%), and 0.25% HA. F. Frequency dependence of G′ and G″ of 5%, 3% and 1.5% G-35-OALG15 gels, and 0.25% HA; G. Amplitude dependence of G′ and G″ of 5%, 3% and 1.5% G-35-OALG15 gels, and 0.25% HA; H. Viscosity as a function of the shear rate for all groups; I. Gelation time of the 5%, 3% and 1.5% G-35-OALG15 gels at 25 ˚C and 37 ˚C, respectively.

observed in all tissue specimens (Fig. 3C). The schematic diagram of subcutaneous degradation experiment in rat was shown in Fig. 3D. The degradation curves were shown in Fig. 3E and F. The degradation rate was fast when G-OALG hydrogel was injected subcutaneously into rat, at day 3, almost no G-OALG hydrogel was left in the implant site and the G-OALG hydrogel could be completely degraded *in vivo* by day 7. The data was described in Table 3. All these results showed G-OALG hydrogel's great histocompatibility.

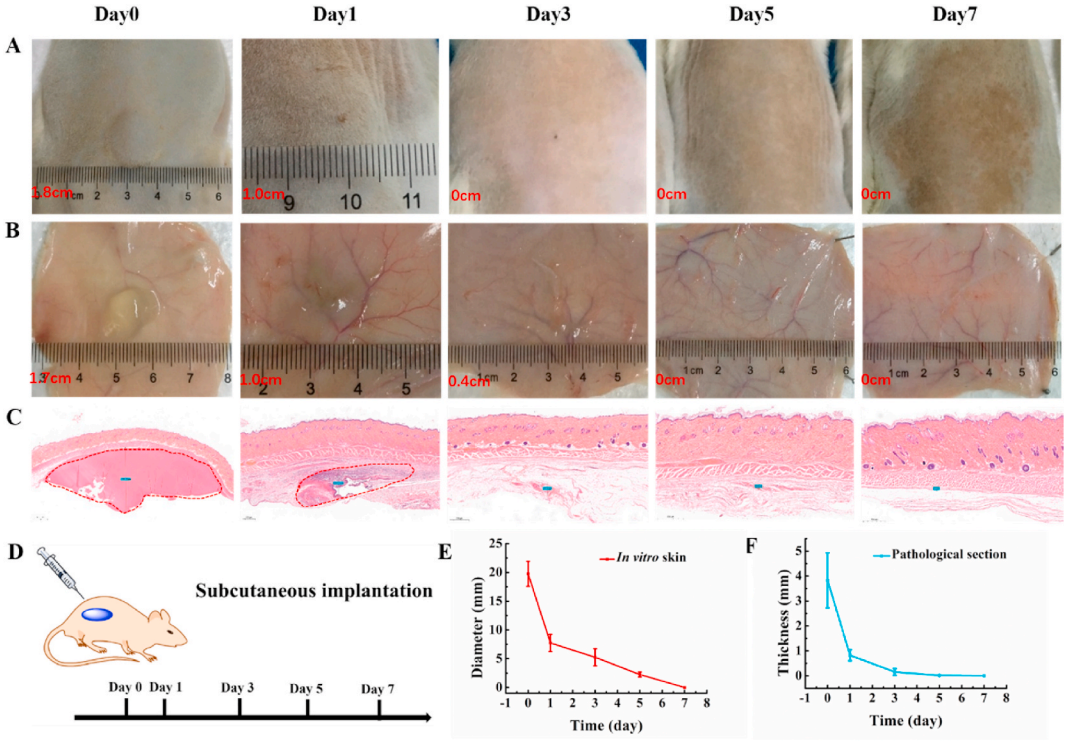

Fig. 3. The degradation in rat experiment. A. The images of injection site on rat at each time point. B. The skin round the injection site was taken for observation at each time point. C. histological analysis. D. The schematic diagram of subcutaneous degradation. E and F. Degradation curve. (n = 4 per group).

Table 3
Degradation in rat at each time points($\bar{x}$ ± SD).

Time(Day)	0	1	3	5	7
Group(n = 4)					
In vivo(diameter)	19.75 ± 2.17	7.75 ± 1.48	5.25 ± 1.48	2.25 ± 0.43	0
Histology(thickness)	3.83 ± 1.10	0.83 ± 0.22	0.16 ± 0.14	0.02 ± 0.00	0

Table 4
The differences among the three materials at each time points($\bar{x}$ ± SD).

Time(min)	1	5	10	20	30	60
Group(n = 3)						
NS	4.60 ± 1.25	3.47 ± 0.76	2.53 ± 0.81	2.27 ± 1.12	1.33 ± 0.61	1.10 ± 0.10
GO1	5.90 ± 1.08	5.23 ± 0.55	4.83 ± 0.29	4.00 ± 0.00	3.77 ± 1.22	3.53 ± 0.71
GO2	7.13 ± 0.12	6.20 ± 1.00	5.90 ± 0.66	5.33 ± 0.42	4.90 ± 0.36	4.40 ± 0.37
P	0.048	0.015	0.002	0.005	0.005	0.000

2.4. Performance of submucosal liquid cushion in pig model

For further evaluating the endoscopic injectability and safety of this gel *in vivo*, we conducted a study on the properties of esophageal submucosal fluid cushion in mini pigs. We firstly compared the characteristics of G-OALG hydrogel with NS in the pig's esophagus.

For NS and GO1 (1.5% G35-OALG15 hydrogel 15 mg/ml), GO2 (5% G35-OALG15 hydrogel 50 mg/ml), 2 ml of each were injected into esophagus submucosa through the endoscopic injection needle, and a good submucosal fluid cushion was formed. The height of the submucosal liquid cushion was observed by endoscope and mini-probe of endoscopic ultrasound (20 MHz EUS) at 1, 5, 10, 20, 30 and 60 min after injection. Endoscopic observation showed that the NS group almost completely diffused out in 10 min after injection, while GO1 and GO2 remained elevated. After 30 min, the GO1 almost was absorbed, while the GO2 remains elevated (Fig. 4). The examination results of EUS were consistent with the endoscopic observation (Fig. 5).

All procedures (Fig. 6A and B) were recorded in Movie S9 (Supplementary information) as shown in Fig. 6A and B. Fig. 6C showed the height of the liquid cushion over time. The height of GO1 and GO2 were better than that of NS group. The heights of GO1 and GO2 were significantly better than that of NS (Table 3). The height of submucosal solution cushion in GO2 group was the best at each time point (Fig. 6D).

Supplementary data related to this article can be found at https://doi.org/10.1016/j.bioactmat.2020.09.028.

2.5. Endoscopy and EUS follow-up

One week later, the esophagus was re-examined by endoscopy and EUS, showing smooth esophageal mucosa without ulceration or erosion

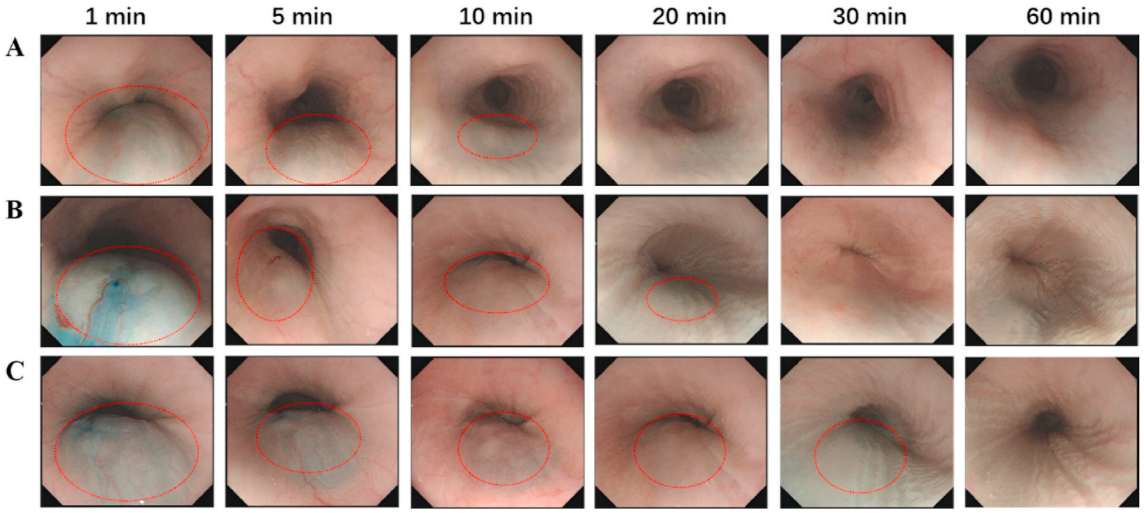

Fig. 4. Submucosal liquid cushions at 1, 5, 10, 20, 30, and 60 min. A. In the NS group, liquid cushions diffused significantly 5 min after injection and were almost completely absorbed 10 min later. B. In the GO1 group, the cushion lasted for 20 min, and it almost completely diffused in 30 min. C. In the GO2 group, the cushion lasted for 30 min, and it almost completely diffused in 60 min. The G-OALG position was marked with red circle.

(Fig. 7). The submucosal liquid cushion in NS and GO1 group has almost been absorbed and could not be found, while submucosal liquid cushion in GO2 group had a very small amount of residue. This result was consistent with the data obtained in rats described above, suggesting that the well degradation rate and histocompatibility was observed.

2.6. Cytotoxicity

The results of the CCK8 assay demonstrated that the infusion of GO-1 andGO-2 hydrogel had extremely low cytotoxicity toward cells (see Fig. 8). These data suggested that infusion of GO hydrogel is suitable for use at the cellular level.

2.7. Biocompatibility in pig

All esophageal tissue specimens were smooth, without erosion and ulcers, and four different sampling sites were identified. (Fig. 9 A, B).H &E staining showed that the submucosal space extended by the injection was free from inflammatory cell infiltration, bleeding and damage in the local tissue in three groups, 2 h after injection (Fig. 9 D, E and F). The submucosal space recovered and only a few inflammatory cells were observed in the local tissue, without erosion, ulcer, fibrous encapsulation and other damages, in three groups, 1 week after injection (Fig. 9 D′, E′, and F′) Local magnification clearly showed a small number of neutrophils scattered in the submucosal fluid cushion (pale blue dots in the red frame) (Fig. 9 D″, E″ and F‴). NS and GO1 were completely absorbed, and a small amount of GO2 with small amounts of inflammatory cells aggregation remained in the submucosa after 1 week (red oval) (Fig. 9 F′, F‴). The results showed that the G-OALG hydrogels had a good biocompatibility.

Most previous studies on submucosal injection have been performed in vitro on the stomach of pigs to observe the duration of the submucosal liquid pad [77–79]. In our study, we not only confirmed that G-OALG hydrogels have an excellent performance for ESD in mini pigs and indicated that it has a good biocompatibility.

3. Conclusions

The G-OALG hydrogels prepared by alginate with sodium periodic oxidation and crosslinking of gelatin and showed excellent endoscopic injectability and gelling performance. The stable water-holding

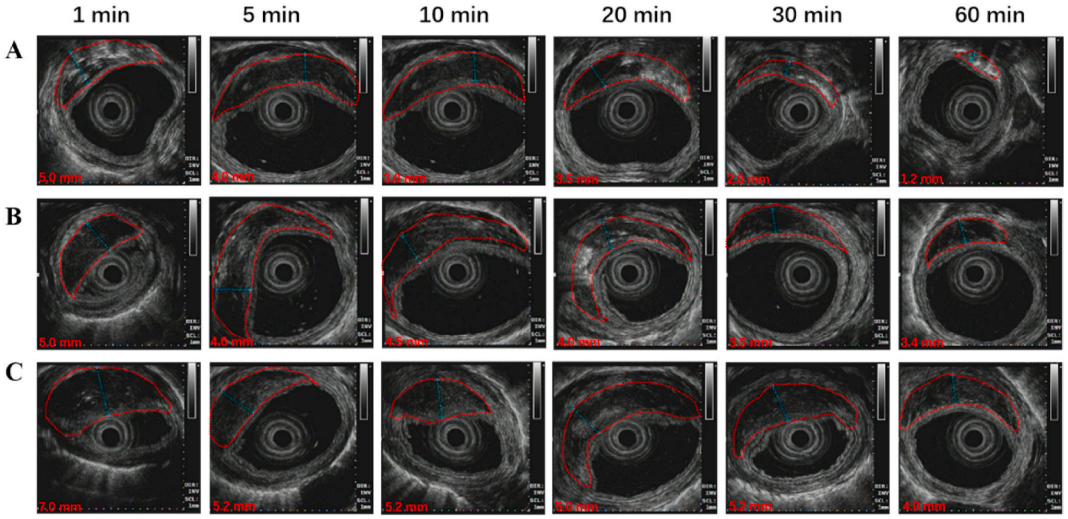

Fig. 5. Endoscopic ultrasonography (EUS) images of the submucosal liquid cushions of NS (A), GO1 (B) and GO2 (C) at different time points (1, 5, 10, 20, 30, 60 min). The G-OALG position was marked with red circle.

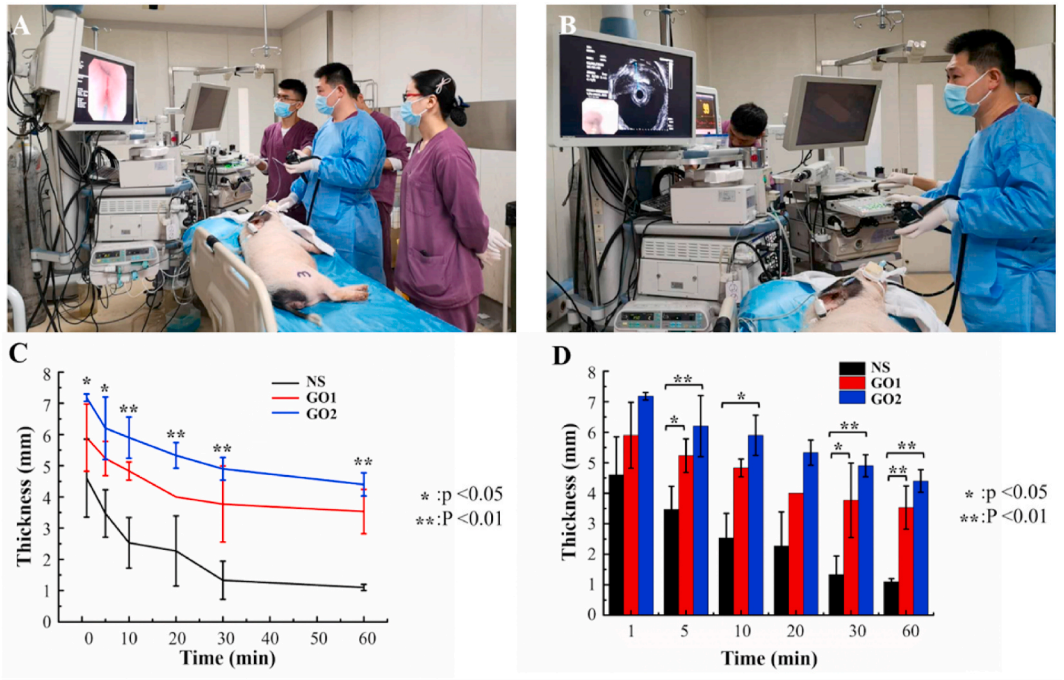

Fig. 6. Experimental process and data analysis. A,B. The procedure of endoscopic injection and EUS examination. C. The differences of height in GO1, GO2 and NS group were analyzed by One-way ANOVA (Table 4). D. The height of submucosal solution cushion changing with the time.

property of the G-OALG hydrogels provide a lasting submucosal liquid cushion height. In addition, the G-OALG hydrogels have non-toxic side effects, good histocompatibility, controllable gelation viscosity and degradation rate, low cost and other advantages. Therefore, the G-OALG hydrogels would well be a promising submucosal injection material for esophageal ESD, STER (submucosal tunnel endoscopic resection), and POEM (per oral endoscopic myotomy), etc.

4. Materials and methods

4.1. 1Basic raw materials

Sodium alginate, and sodium metaperiodate (98%) were purchased from Alfa Aesar (A Johnson Matthey Company). Gelatin was purchased from Ward's Science (Rochester, NY). Ethylene glycol (≥99%) was supplied by VWR International, LLC. All chemicals were used as received.

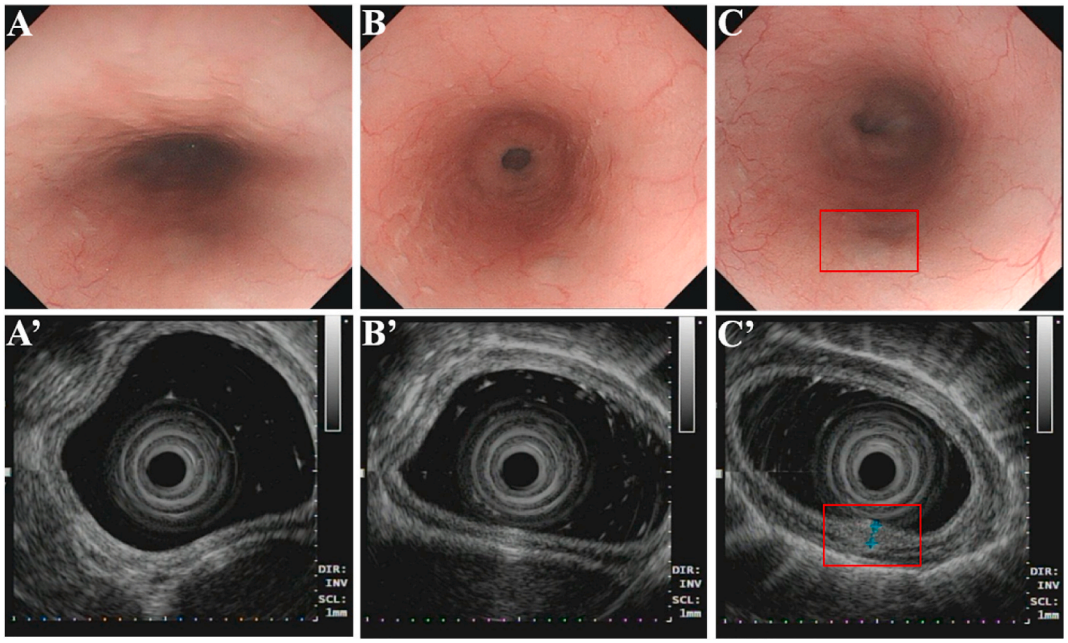

Fig. 7. Endoscopic and EUS images of the submucosal liquid cushions developed after 1 week. The endoscopic images of submucosal liquid cushion in NS (A), GO1 (B) and GO2 (C). The submucosal liquid cushion in GO2 group remained little of residue (Red frame). The EUS images of submucosal liquid cushion in NS (A′), GO1 (B′) and GO2 (C′).

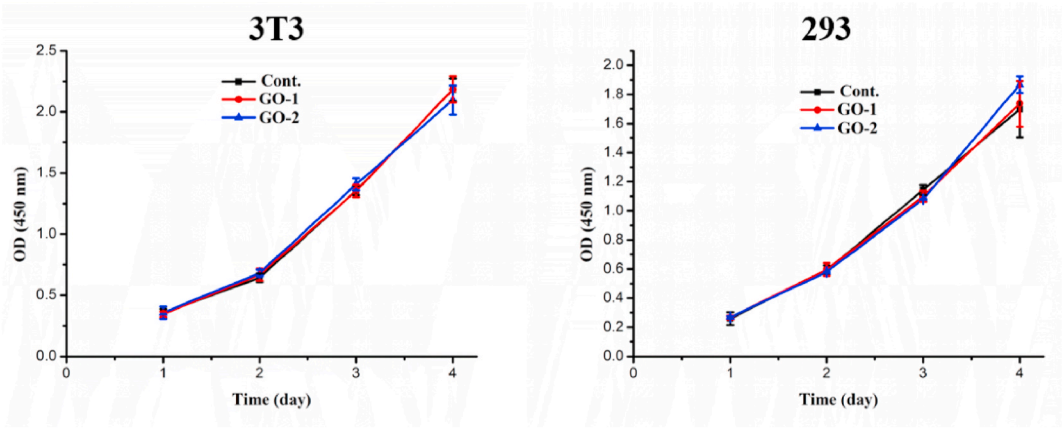

Fig. 8. Evaluation of **in vitro** biocompatibility of GO with live cell cultures. The cytotoxicity of this hydrogel to 3T3 and 293 fibroblasts after incubation for 1, 2, 3 and 4 days. (n = 3 per group).

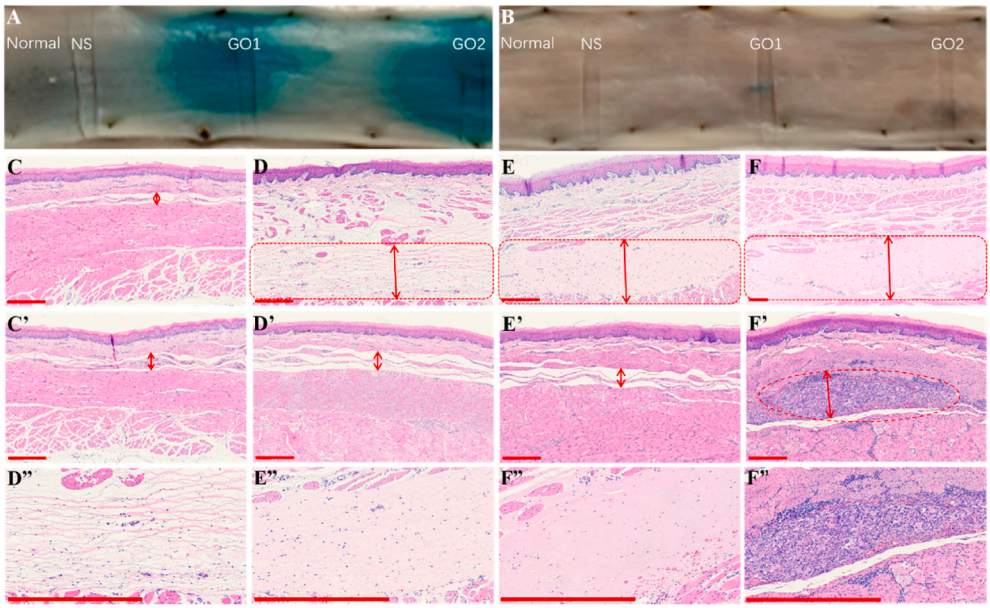

Fig. 9. Esophageal tissue specimens were smooth, without erosion and ulcers, and four different sampling sites (Normal, NS, GO1 and GO2) were identified. A. 2 h after injection. B. 1 week after injection. H&E staining showed no significant inflammatory infiltration and fibrosis. The red two-way arrow and red frame represents the thickness and extent of the submucosal space. C, C'. Normal esophagus; D, E, and F. The histopathological images of NS, GO1 and GO2 group after 2 h injection. D′, E′, and F'. The histopathological images of NS, GO1 and GO2 group after 1 week injection. D″, E″, F″ and F‴. The images representing D, E, F and F'. are further enlarged. Red scale bar, 300 μm.

4.2. Preparation of hydrogels

4.2.1. The first step: Preparation of oxidized alginate (OALG)

The OALG was prepared by reacting sodium alginate with sodium metaperiodate using a modification. Briefly, 1.5 g sodium alginate was dissolved in 75 ml deionized water to obtain an alginate solution with a concentration of 2% (w/v), 0.75 g sodium metaperiodate was dissolved into 5 ml deionized water and then added to the alginate solution dropwise. The oxidation reaction proceeded thoroughly in the dark by magnetic stirring for 24 h at room temperature. The 1 ml ethylene glycol was added to terminate the oxidization and stirred for another 2 h at room temperature. The reaction solution was dialyzed against deionized water for 3 days and lyophilization to obtain solid OALG, and stored in −20 ˚C for further use.

4.2.2. The second step: Preparation of gelatin-OALG (G-OALG) hydrogels

The hydrogels were prepared by mixing prepared gelatin solution and OALG solution with different proportions. Briefly, gelatin solutions (3%, 4%, 5%, 6%, 7%, 8% (w/v)) and OALG solutions (2%, 3%, 4%, 5%, 6%, 7% (w/v)) with different concentrations were prepared by dissolving gelatin and OALG in deionized water in advance; then, gelatin solution and OALG solution were mixed together to form crosslinked G-OALG hydrogels; the weight ratios of gelatin to OALG in final hydrogels were 40:10, 35:15, 30:20, 25:25, 20:30, and 30:70, their compositions are shown in Table 2. To prepare the G35-OALG15 gels with concentrations of 1.5% (w/v) and 3% (w/v), the 1.5% and 3% gelatin solution, and OALG solutions were first prepared, respectively. Then, 1.5% or 3% gelatin solution, and 1.5% or 3% OALG solution were mixed, respectively, to form crosslinked G35-OALG15 hydrogels with weight ratio of gelatin to OALG was 35:15 in final gels.

4.3. FTIR analysis

A Nicolet iS10 Fourier transform infrared (FTIR) spectrometer was used to evaluate the crosslinking between gelatin and OALG, and 64 scan per sample with a resolution of 4. Lyophilized G35-OALG15 hydrogel, OALG, and powders of gelatin and alginate were used to record Fourier transform infrared (ATR-FTIR) spectra.

4.4. Rheological analysis

A TA Discovery HR1 hybrid rheometer was used for the rheological analysis of the G-OALG hydrogels. A steel cone plate geometry with a cone diameter of 20 mm and a cone angle of 2˚ was used. The oscillation time sweep experiment was performed to record the storage modulus (G′) and loss modulus (G″) of mixed sample solutions to

achieve the crosslinking points of G35-OALG15 hydrogels at 25 ˚C as strain and angular frequency were set up as 0.5% and 10.0 rad/s, respectively. For the oscillation time sweep experiment of G35-OALG15 at 37 ˚C, both gelatin solution and OALG solution were first incubated at 37 ˚C water baths. Samples were placed on the plate immediately after mixing. Rheological studies of all groups' hydrogels (G-OALG hydrogels with different composites and G35-OLAG15 gels of different concentrations), and 0.25% HA were analyzed at 25 ˚C. Shear viscosity data of all groups' hydrogels and 0.25% HA were measured and compared; the shear rate was increased from 1.0e-3 to 2.0e3 1/s. Dynamic frequency sweep measurements of G-OALG hydrogel with different composites and G35-OLAG15 gels of different concentrations, and 0.25% HA were recorded under the angular frequency was from 0.1 to 100.0 rad/s at strain of 0.5%. Amplitude logarithmic sweep measurement of all samples were conducted with strain vary from 1.0e-1% to 2.0e3% at angular frequency of 10.0 rad/s.

4.5. Nuclear magnetic resonance (NMR) analysis

^{1}H NMR spectra of alginate and OALG samples were characterized by an Advanced 300 spectrometer. Samples were dissolved in deuterium oxide (D_2O) with a concentration of 10 mg/ml (1 w/v%), respectively.

4.6. Gelation time of the hydrogels

The vial inverting method was used to determine the gelation time at 25 ˚C. Briefly, gelatin solution was slowly added to OALG solution within a glass vessel and keep stirring. Chemical binding between gelatin and OALG occurred during crosslinking. The gelation time was recorded as the hydrogel stopped flowing by inverting the vessel and observing at room temperature. The magnetically stir bar stirring method was used to determine the gelation time at 37 ˚C. Briefly, gelatin solution and OALG solution were mixed in a glass vessel and keep stirring magnetically at 37 ˚C oil baths. The time was recorded as the stirring bar was stopped. All experiments have been taken in three times.

4.7. Biocompatibility testing in rats

Male rats (Chongqing, China, License No.: SYXK 2017-0010), weight of 200–250 g each, were used in the *in vivo* degradation studies. All animal experiments complied with the Guide for the Care and Use of Laboratory Animals published by the US National Institutes of Health, and approved by the Laboratory Animal Welfare and Ethics Committee of Third Military Medical University (No. AMUWEC20191278). Hydrogel samples (C = 50 mg/ml, methylene blue concentration 0.01%) were injected in the mediodorsal skin under sterile conditions. At designated time intervals (days of 1, 3, 5, and 7), the rats were sacrificed and the samples were processed for histological analyses and biodegradation studies. Methods for measuring residual hydrogels at different time points in animal models. After we anesthetized and killed the mice, we removed the skin from the back of the mice and measured the diameter of the protrusion with a ruler. In the pathological sections, we tested the thickness of the hydrogel with software. Four rats in each group were tested in parallel.

4.8. Endoscopic process in mini pigs

The experimental procedures in this study were approved by the Laboratory Animal Welfare and Ethics Committee of Third Military Medical University (No. AMUWEC20191278). In total, three female Bama mini pigs (Chongqing, China, License No.: SYXK 2017-0010), weight of 20–25 kg each, were observed for *in vivo* experiments. Through clinical observation and blood tests (blood routine, liver and kidney function), all pigs were in healthy condition. Two days before the experiment, each pig was allowed to drink water only. When the pigs were anesthetized by Xylazine Hydrochloride (HuaMu animal health products co. Ltd. Jilin, China.) and Propofol (LIBANG Pharmaceutical Co. Ltd. Xi' an, China), endotracheal intubation was performed with continuous oxygen intake of 2 L per minute. Next, the endoscope (Olympus Corp, Tokyo, Japan.) entered into the pig's esophagus for the observation, and NS, GO1and GO2, 2 ml of each (methylene blue concentration 0.01%), were injected, respectively, into the submucosa with an endoscopic needle (23G, 2.3m-long, Boston, Scientific Corp, Boston, America.) at 15 cm, 10 cm and 5 cm above the esophagogastric junction. The thickness of submucosal liquid cushion was observed by endoscopy and 20 MHz EUS (Olympus Corp, Tokyo, Japan.) at 1, 5, 10, 20, 30, and 60 min after the injection. The obtained images and data were recorded and analyzed.

4.9. Proliferation assay

3T3 and 293 fibroblasts cells were purchased from the Cell bank of the Chinese Academy of Sciences. The proliferation of 3T3 and 293 cells were assessed by the Counting Kit-8 (CCK-8) method. Briefly, 3T3 and 293 cells were seeded into 96-well plates with a density of 1000 cells/100 μL/well and incubated for 24 h at 37 ˚C in a 5% CO2 humidified incubator to obtain a monolayer of cells. The GO hydrogel extract was used to replace the cell culture medium and the cells were incubated for 1, 2, 3 and 4 days. Remove the solution of sample and added 90 μL fresh medium (10 μL CCK-8 reagent) to each well, and incubate at 37 ˚C for 2 h. The absorbance of the sample was measured by a microplate reader (SpectraMax 190, USA) at 450 nm. Five independent cultures were prepared for each sample, and the proliferation assays of each culture was repeated for 3 times.

4.10. Biocompatibility tests in mini pigs

Five mini pigs were used for biocompatibility testing. Two of the pigs were euthanized 2 h after submucosal injection and three were euthanized 1 week after submucosal injection. These esophageal tissues were taken out and soaked in 10% formalin solution for 48 h, and then the tissues at the injection site were selected for histological analyses and biodegradation studies.

4.11. Statistical analysis

SPSS22.0 (IBM) was used for statistic of this study. Continuous variables were presented as mean ± SD. One-way ANOVA analysis was used for variable within the groups. Further pairwise comparisons were performed by the Tamhane's TM(2). p-value of less than 0.05 was considered statistically significant.

Author contribution

Shiming Yang and Malcolm Xing: Conception and Writing- reviewing and editing.

Chaoqiang Fan: ESD pig animal and other in vivo test, writing the manuscript.

Kaige Xu: Materials synthesis and characterization, writing the manuscript.

Yu Huang: hydrogel in pig submucosal, biocompatibility tests, writing the manuscript.

Shuang Liu: in vivo experiments and data analysis.

Tongchuan Wang: Cell culture and toxicity analysis.

Wei Wang: anesthesiologist in administering anesthesia to laboratory animals.

Weichao Hu: subcutaneous implantation, data collation, analysis.

Lu Liu: Assist to complete in vivo experiments and histo-pathological observation.

Data availability

The raw and processed data required to reproduce the results are available from the authors.

Declaration of competing interest

None of the authors of this manuscript has a conflict of interest.

Acknowledgements

This work was supported by grants from the the National Science Foundation of China (No.81802982), and ChongQing Science & Technology Commission Fund (No. CSTC2018jcyjAX0102).

Appendix A. Supplementary data

Supplementary data to this article can be found online at https://doi.org/10.1016/j.bioactmat.2020.09.028.

References

[1] S.G. Thrumurthy, et al., Oesophageal cancer: risks, prevention, and diagnosis, BMJ 366 (2019) l4373.
[2] F. Bray, et al., Global cancer statistics 2018: GLOBOCAN estimates of incidence and mortality worldwide for 36 cancers in 185 countries, Ca - Cancer J. Clin. 68 (6) (2018) 394–424.
[3] M. Takuji Gotoda, M.D. Hitoshi Kondo, Hiroyuki Ono, M.D. Yutaka Saito, M.D. Hajime Yamaguchi, M.D. Daizo Saito, M.D. Toshihiro Yokota, A new endoscopic mucosal resection procedure using an insulation-tipped electrosurgical knife for rectal flat lesions: report of two cases, Gastrointest. Endosc. 50 (1999) 560–563.
[4] P.V. Draganov, et al., AGA institute clinical practice update: endoscopic submucosal dissection in the United States, Clin. Gastroenterol. Hepatol. 17 (1) (2019) 16–25.
[5] A.T. Committee, et al., Endoscopic submucosal dissection, Gastrointest. Endosc. 81 (6) (2015) 1311–1325.
[6] A.O. Ferreira, et al., Solutions for submucosal injection in endoscopic resection: a systematic review and meta-analysis, Endosc. Int. Open 4 (1) (2016) E1–E16.
[7] H. Yandrapu, et al., Normal saline solution versus other viscous solutions for submucosal injection during endoscopic mucosal resection: a systematic review and meta-analysis, Gastrointest. Endosc. 85 (4) (2017) 693–699.
[8] Y. Matsui, et al., Hyaluronic acid stimulates tumor-cell proliferation at wound sites, Gastrointest. Endosc. 60 (4) (2004) 539–543.
[9] M. Fujishiro, et al., Tissue damage of different submucosal injection solutions for EMR, Gastrointest. Endosc. 62 (6) (2005) 933–942.
[10] K. Fasoulas, et al., Endoscopic mucosal resection of giant laterally spreading tumors with submucosal injection of Hydroxyethyl starch: comparative study with normal saline solution, Surg. Laparosc. Endosc. Percutaneous Tech. 22 (3) (2012) 272–278.
[11] D.K. Rex, et al., SIC-8000 versus hetastarch as a submucosal injection fluid for EMR: a randomized controlled trial, Gastrointest. Endosc. 90 (5) (2019) 807–812.
[12] T. Uraoka, et al., Submucosal injection solution for gastrointestinal tract endoscopic mucosal resection and endoscopic submucosal dissection, Drug Des. Dev. Ther. 2 (2009) 131–138.
[13] Y.S. Jung, D.I. Park, Submucosal injection solutions for endoscopic mucosal resection and endoscopic submucosal dissection of gastrointestinal neoplasms, Gastroint. Intervent. 2 (2) (2013) 73–77.
[14] A. Moss, M.J. Bourke, A.J. Metz, A randomized, double-blind trial of succinylated gelatin submucosal injection for endoscopic resection of large sessile polyps of the colon, Am. J. Gastroenterol. 105 (11) (2010) 2375–2382.
[15] S.H. Lee, et al., A new method of EMR: submucosal injection of a fibrinogen mixture, Gastrointest. Endosc. 59 (2) (2004) 220–224.
[16] M. Pioche, et al., High-pressure jet injection of viscous solutions for endoscopic submucosal dissection: a study on ex vivo pig stomachs, Surg. Endosc. 28 (5) (2014) 1742–1747.
[17] Y.M. Shastri, et al., Autologous blood as a submucosal fluid cushion for endoscopic mucosal therapies: results of an ex vivo study, Scand. J. Gastroenterol. 42 (11) (2007) 1369–1375.
[18] W. Wen, et al., A pilot animal and clinical study of autologous blood solution compared with normal saline for use as an endoscopic submucosal cushion, Exp. Ther. Med. 4 (3) (2012) 419–424.
[19] I. Kumano, et al., Endoscopic submucosal dissection for pig esophagus by using photocrosslinkable chitosan hydrogel as submucosal fluid cushion, Gastrointest. Endosc. 75 (4) (2012) 841–848.
[20] H.T. Hattori, H. Tsujimoto, K. Hase, M. Ishihara, Characterization of a water-soluble chitosan derivative and its potential for submucosal injection in endoscopic techniques, Carbohydr. Polym. 175 (2017) 592–600.
[21] L. Yu, et al., Poly(lactic acid-co-glycolic acid)–poly(ethylene glycol)–poly(lactic acid-co-glycolic acid) thermogel as a novel submucosal cushion for endoscopic submucosal dissection, Acta Biomater. 10 (3) (2014) 1251–1258.
[22] S.H. Eun, et al., Effectiveness of sodium alginate as a submucosal injection material for endoscopic mucosal resection in animal, Gut and Liver 1 (1) (2007) 27–32.
[23] T. Akagi, et al., Sodium alginate as an ideal submucosal injection material for endoscopic submucosal resection: preliminary experimental and clinical study, Gastrointest. Endosc. 74 (5) (2011) 1026–1032.
[24] N. Uemura, et al., Efficacy and safety of 0.6% sodium alginate solution in endoscopic submucosal dissection for esophageal and gastric neoplastic lesion: a randomized controlled study, Dig. Endosc. 31 (4) (2019) 396–404.
[25] K.J. Kang, et al., Alginate hydrogel as a potential alternative to hyaluronic acid as submucosal injection, Mater. Dige. Dis. Sci. 58 (6) (2013) 1491–1496.
[26] H. Yamamoto, et al., Successful en-bloc resection of large superficial tumors in the stomach and colon using sodium hyaluronate and small-caliber-tip transparent hood, Endoscopy 35 (8) (2003) 690–694.
[27] M. Fujishiro, et al., Successful outcomes of a novel endoscopic treatment for GI tumors: endoscopic submucosal dissection with a mixture of high-molecular-weight hyaluronic acid, glycerin, and sugar, Gastrointest. Endosc. 63 (2) (2006) 243–249.
[28] N. Yoshida, et al., Endoscopic mucosal resection with 0.13% hyaluronic acid solution for colorectal polyps less than 20 mm: a randomized controlled trial, J. Gastroenterol. Hepatol. 27 (8) (2012) 1377–1383.
[29] M.M. Islam, et al., Chitosan based bioactive materials in tissue engineering applications-A review, Bioactive Mater. 5 (1) (2020).
[30] B. Xin, et al., Bioactive hydrogels for bone regeneration, Bioactive Mater. 3 (4) (2018) 401–417.
[31] H. Zhang, et al., Recent advances of two-dimensional materials in smart drug delivery nano-systems, Bioactive Mater. 5 (4) (2020) 1071–1086.
[32] H. Hecht, S. Srebnik, Structural characterization of sodium alginate and calcium alginate, Biomacromolecules 17 (6) (2016) 2160–2167.
[33] S.J. Jeon, A.W. Hauser, R.C. Hayward, Shape-morphing materials from stimuli-responsive hydrogel hybrids, Acc. Chem. Res. 50 (2) (2017) 161–169.
[34] J. Leppiniemi, et al., 3D-Printable bioactivated nanocellulose-alginate hydrogels, ACS Appl. Mater. Interfaces 9 (26) (2017) 21959–21970.
[35] Jung, #79;Kumano, 2012 #738;Islam, (2013), p. 794 2020.
[36] X.Y. Geng, O.H. Kwon, J.H. Jang, Electrospinning of chitosan dissolved in concentrated acetic acid solution, Biomaterials 26 (27) (2005) 5427–5432.
[37] N.R. Hosseini, J.S. Lee, Biocompatible and flexible chitosan-based resistive switching memory with magnesium electrodes, Adv. Funct. Mater. 25 (35) (2015) 5586–5592.
[38] X.H. Wang, et al., Crosslinked collagen/chitosan matrix for artificial livers, Biomaterials 24 (19) (2003) 3213–3220.
[39] Y. Pang, et al., Endoscopically injectable shear-thinning hydrogels facilitating polyp removal, Adv. Sci. 6 (19) (2019) 1901041.
[40] R. Castro, et al., Solutions for submucosal injection: what to choose and how to do it, World J. Gastroenterol. 25 (7) (2019) 777–788.
[41] J.W. Nichol, et al., Cell-laden microengineered gelatin methacrylate hydrogels, Biomaterials 31 (21) (2010) 5536–5544.
[42] J.M. Zhu, R.E. Marchant, Design properties of hydrogel tissue-engineering scaffolds, Expet Rev. Med. Dev. 8 (5) (2011) 607–626.
[43] M.A. Daniele, et al., Interpenetrating networks based on gelatin methacrylamide and PEG formed using concurrent thiol click chemistries for hydrogel tissue engineering scaffolds, Biomaterials 35 (6) (2014) 1845–1856.
[44] P. Amrita, B.L. Vernon, N. Mehdi, Therapeutic neovascularization promoted by injectable hydrogels, Bioactive Mater. 3 (4) (2018) 389–400.
[45] O. Mahony, et al., Silica-gelatin hybrids with tailorable degradation and mechanical properties for tissue regeneration, Adv. Funct. Mater. 20 (22) (2010) 3835–3845.
[46] S.T. Koshy, et al., Injectable, porous, and cell-responsive gelatin cryogels, Biomaterials 35 (8) (2014) 2477–2487.
[47] B. Balakrishnan, et al., Evaluation of an in situ forming hydrogel wound dressing based on oxidized alginate and gelatin, Biomaterials 26 (32) (2005) 6335–6342.
[48] T. Hozumi, et al., Injectable hydrogel with slow degradability composed of gelatin and hyaluronic acid cross-linked by schiff's base formation, Biomacromolecules 19 (2) (2018) 288–297.
[49] C.G. Gomez, M. Rinaudo, M.A. Villar, Oxidation of sodium alginate and characterization of the oxidized derivatives, Carbohydr. Polym. 67 (3) (2007) 296–304.
[50] D. Heo, et al., 3D Bioprinting of carbohydrazide-modified gelatin into microparticle-suspended oxidized alginate for fabrication of complex-shaped tissue constructs, ACS Appl. Mater. Interfaces 12 (18) (2020) 20295–20306.
[51] B. Sarker, et al., Fabrication of alginate–gelatin crosslinked hydrogel microcapsules and evaluation of the microstructure and physico-chemical properties, J. Mater. Chem. B 2 (11) (2014) 1470–1482.
[52] B. Balakrishnan, et al., Self-crosslinked oxidized alginate/gelatin hydrogel as injectable, adhesive biomimetic scaffolds for cartilage regeneration, Acta Biomater. 10 (8) (2014) 3650–3663.
[53] H. Liao, H. Zhang, W. Chen, Differential physical, rheological, and biological properties of rapid in situ gelable hydrogels composed of oxidized alginate and gelatin derived from marine or porcine sources, J. Mater. Sci. Mater. Med. 20 (6) (2009) 1263–1271.
[54] L.S. Guinesi, É.T.G. Cavalheiro, Influence of some reactional parameters on the substitution degree of biopolymeric Schiff bases prepared from chitosan and salicylaldehyde, Carbohydr. Polym. 65 (4) (2006) 557–561.
[55] C. Joly-Duhamel, D. Hellio, M. Djabourov, All gelatin networks: 1. Biodiversity and physical chemistry, Langmuir 18 (19) (2002) 7208–7217.
[56] L. Ghasemi-Mobarakeh, et al., Electrospun poly(epsilon-caprolactone)/gelatin nanofibrous scaffolds for nerve tissue engineering, Biomaterials 29 (34) (2008) 4532–4539.
[57] Q.Y. He, Y. Huang, S.Y. Wang, Hofmeister effect-assisted one step fabrication of ductile and strong gelatin hydrogels, Adv. Funct. Mater. 28 (5) (2018).
[58] S.K. Tam, et al., Physicochemical model of alginate–poly-l-lysine microcapsules

defined at the micrometric/nanometric scale using ATR-FTIR, XPS, and ToF-SIMS, Biomaterials 26 (34) (2005) 6950–6961.
[59] Y.P. Wang, et al., Controlled drug release from a novel drug carrier of calcium polyphosphate/chitosan/aldehyde alginate scaffolds containing chitosan microspheres, RSC Adv. 4 (47) (2014) 24810–24815.
[60] Z. Yu, et al., Two-dimensional FTIR spectroscopic characterization of functional groups of NaOCl-exposed alginate: insights into membrane refouling after online chemical cleaning, ACS Appl. Bio Mater. 1 (3) (2018) 593–603.
[61] C.K. Song, et al., Dopa-empowered Schiff base forming alginate hydrogel glue for rapid hemostatic control, Macromol. Res. 27 (2) (2019) 119–125.
[62] E.F.S. Vieira, et al., Polysaccharide-based hydrogels: Preparation, characterization, and drug interaction behaviour, Biomacromolecules 9 (4) (2008) 1195–1199.
[63] J. Brus, et al., Structure and dynamics of alginate gels cross-linked by polyvalent ions probed via solid state NMR spectroscopy, Biomacromolecules 18 (8) (2017) 2478–2488.
[64] L. Wang, et al., Preparation and catalytic performance of alginate-based Schiff Base, Carbohydr. Polym. 208 (2019) 42–49.
[65] J. Dahlmann, et al., Fully defined in situ cross-linkable alginate and hyaluronic acid hydrogels for myocardial tissue engineering, Biomaterials 34 (4) (2013) 940–951.
[66] Y.S. Zhang, A. Khademhosseini, Advances in engineering hydrogels, Science 356 (6337) (2017).
[67] Z. Munoz, H. Shih, C.C. Lin, Gelatin hydrogels formed by orthogonal thiol-norbornene photochemistry for cell encapsulation, Biomater. Sci. 2 (8) (2014) 1063–1072.
[68] E.I. Wisotzki, et al., Magnetic response of gelatin ferrogels across the sol-gel transition: the influence of high energy crosslinking on thermal stability, Soft Matter 12 (17) (2016) 3908–3918.
[69] F.C. Marisa Erencia, Jose A. Tornero, Margarida M. Fernandes, Tzanko Tzanov, Jorge Macanas, Fernando Carrillo, Electrospinning of gelatin fibers using solutions with low acetic acid concentration: effect of solvent composition on both diameter of electrospun fibers and cytotoxicity, J. Appl. Polym. Sci. (2015) 1–11.
[70] Y.C. Jiang, et al., Electrospun polycaprolactone/gelatin composites with enhanced cell-matrix interactions as blood vessel endothelial layer scaffolds, Mater. Sci. Eng. C-Mater. Biol. Appl. 71 (2017) 901–908.
[71] S.H. Lee, et al., Clinical efficacy of EMR with submucosal injection of a fibrinogen mixture: a prospective randomized trial, Gastrointest. Endosc. 64 (5) (2006) 691–696.
[72] S. Bajpai, M. Bajpai, F.F. Shah, Alginate dialdehyde (AD)-crosslinked casein films: synthesis, characterization and water absorption behavior, Des. Monomers Polym. 19 (5) (2016) 406–419.
[73] Z. Emami, et al., Controlling alginate oxidation conditions for making alginate-gelatin hydrogels, Carbohydr. Polym. 198 (2018) 509–517.
[74] B. Balakrishnan, A. Jayakrishnan, Self-cross-linking biopolymers as injectable in situ forming biodegradable scaffolds, Biomaterials 26 (18) (2005) 3941–3951.
[75] H. Yandrapu, et al., Normal saline solution versus other viscous solutions for submucosal injection during endoscopic mucosal resection: a systematic review and meta-analysis, Gastrointest. Endosc. 85 (4) (2017) 693–699.
[76] R. Hirose, et al., Development of sodium polyacrylate-based high-performance submucosal injection material with pseudoplastic fluid characteristics, ACS Biomater. Sci. Eng. 5 (12) (2019) 6794–6800.
[77] T. Uraoka, et al., Carbon dioxide submucosal injection cushion: an innovative technique in endoscopic submucosal dissection, Dig. Endosc. 23 (1) (2011) 5–9.
[78] O.H. Al-Taie, et al., Efficacy of submucosal injection of different solutions inclusive blood components on mucosa elevation for endoscopic resection, Clin. Exp. Gastroenterol. 5 (2012) 43–48.
[79] N. Mehta, et al., Optimal injection solution for endoscopic submucosal dissection: a randomized controlled trial of Western solutions in a porcine model, Dig. Endosc. 30 (3) (2018) 347–353.